Railway ballast layer inspection with different GPR antennas and frequencies

Liu, Guixian; Peng, Zhan; Jing, Guoqing; Wang, Shilei; Li, Yaonan; Guo, Yunlong

DOI
10.1016/j.trgeo.2022.100823

Publication date
2022

Document Version
Final published version

Published in
Transportation Geotechnics

Transportation Geotechnics 36 (2022) 100823

Contents lists available at ScienceDirect

Transportation Geotechnics

journal homepage: www.elsevier.com/locate/trgeo

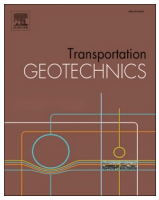

Railway ballast layer inspection with different GPR antennas and frequencies

Guixian Liu [a], Zhan Peng [a], Guoqing Jing [b], Shilei Wang [a], Yaonan Li [a], Yunlong Guo [c,*]

[a] Infrastructure Inspection Research Institute, China Academy of Railway Sciences Co., Ltd., Beijing 100081, China
[b] School of Civil Engineering, Beijing Jiaotong University, Beijing 100044, China
[c] Faculty of Civil Engineering and Geosciences, Delft University of Technology, Delft 2628CN, Netherlands

ARTICLE INFO

Keywords:
Ground penetrating radar
GPR
Railway ballast
Track inspection
Ballast fouling
Track geometry

ABSTRACT

Ground penetrating radar (GPR) is a popular technology for inspecting railway ballast layer, mainly on the ballast fouling level. However, different GPR antennas with different frequencies are suitable for different inspection emphasis and diverse railway lines (weather and sub-structure). In addition, the full-scale track model (with subgrade) for experimental tests was not seen in earlier studies. For further application of GPR in China, the GPR inspections (with 400 MHz, 900 MHz and 2 GHz antennas) were performed on a 30 m long full-scale track and three railway lines (different weather and sub-structure). Results show that ballast layer inspection should be performed mainly with the 2 GHz antenna and supplemented by the 400 MHz and 900 MHz antennas. The weather has great influence on the results of GPR inspection. This study is helpful for supplementing the guidance of ballast layer inspection with GPR.

Introduction

Ballast layer is the crucial component for the ballasted track [1]. Ballast layer differential deformation very likely results in track irregularity [2,3]. Under the train cyclic loadings after long service time, the ballast layer differential deformation possibility gradually increases, and meanwhile the ballast layer gradually loses its elasticity and drainage [4–6]. The track geometry is maintained by frequent maintenance work (tamping, stabilisation), and eventually the ballast cleaning and renewal must be performed [7–9].

Ballasted track performance is mostly determined by the ballast layer condition [10], while fouling (also named as contamination) in ballast layer is a key factor to determine the ballast layer condition [11,12]. In addition, ballast fouling and degradation is the reason why ballast layer needs to be cleaned and replaced by new ballast [13,14]. Even so, due to the limited development of track inspection equipment and technology [15,16], current ballast layer condition is mostly assessed by indirect means through the total passing gross load [7–9].

In the earlier studies, two means were used to inspect ballast layer. Visual inspection is the most common one, which is quite subjective. Usually, when the mud-pumping [17] occurs, then we know ballast layer is highly fouled [18]. Field ballast layer drilling is another traditional means to evaluate ballast layer condition, mainly to obtain the fouling index by sieving the fouled sample [19,20]. This means is expensive and intrusive. The ground penetrating radar (GPR) is considered to be the rapid and effective technology for ballast layer condition evaluation, although at the beginning stage [21].

GPR is a non-destructive inspection technique. It was applied in many studies to evaluate ballast layer condition [22]. Almost all the studies related with GPR application on ballast layer is quantifying the ballast fouling, and correlating the GPR fouling index with sieving fouling index [23–29]. A few studies were on the GPR signal characteristics and processing means [21,30–34]. Several reports from Transportation Technology Center, Inc. and plenty of studies demonstrated the GPR application on the field [35–47]. Specifically, these multiple studies can be summarised and classified into the following aspects.

Dielectric constant of ballast layer is used to evaluate ballast fouling level. Clean ballast particles were mixed with soil, which simulates fouled ballast layer. Different mass percentages (0 % – 24 %) of soil were mixed in ballast layer. The corresponding dielectric constants are 3.51 to 5.35 (0 % – 24 % soil) [25]. Dielectric constants of fouled ballast layer were also measured in [28]. Two kinds of fouling were used, i.e. sands and gravel. Different fouling percentages (0 % – 50 %) were mixed in ballast layer. Results show that the dielectric constant can

* Corresponding author.
E-mail address: Yunlong.guo@tudelft.nl (Y. Guo).

https://doi.org/10.1016/j.trgeo.2022.100823
Received 20 January 2022; Received in revised form 29 June 2022; Accepted 25 July 2022
Available online 29 July 2022

reflect ballast fouling level. But one measured dielectric constant has many possibilities, e.g., fouling sources and water content [48]. Moreover, the dielectric contact is calculated through the ballast layer thickness, which is usually not known in the field railway line. The desired results cannot be obtained, e.g. the fouling sources, water content and ballast layer thickness. To obtain these desired results, in-situ ballast layer drilling and sieving are still needed.

GPR signal processing means were developed to evaluate ballast fouling. Time-domain GPR signal is normally obtained from the GPR equipment. Using the Fourier transform, the time-domain GPR signal is converted into frequency-domain signal, which can more clearly show ballast fouling level [45]. New GPR signal processing means was proposed in [21] using time-domain signal. Four indicators were created, including featuring area, axis crossing and inflexion point. It was proposed in [34] using wavelet transform to process the GPR signal (time-domain). Both time-domain and frequency-domain signal processing means were applied in [46].

A linear correlation was created between the indicator (GPR signal analysis result) and the fouling level based on the low frequency GPR signal around 500 MHz, while the relationship based on the medium and high frequency antenna at 1–2 GHz tends to be more complex and shows a high regression phenomenon. This phenomenon may also result from the limited number of samples. GPR signals were collected mostly in dry field or indoor environment, and the GPR signals of the water-containing ballast layer in the natural environment are not yet correlated with the fouling level. In order to ensure the applicability of the GPR, the relationship between the GPR signal and the radar signal indicator needs to be established in conjunction with the ballast grading (particle size distribution; PSD) and railway line type, considering different calculation methods of ballast degradation and fouling index in different countries, such as ballast material and PSD [7–9,49].

The large number of studies have proved that the ability of GPR on ballast layer detection/inspection. The general conclusion is that high-frequency antennas (2 GHz) are more suitable for ballast layer condition detection. Low-frequency and medium-frequency antennas (400 MHz) can be used for distinguishing ballast-subgrade interface. The earlier studies show the direction of suitable antennas for our work.

In this paper, a 30 m full-scale ballasted track was built with different percentages of fouling mixed in its ballast layer in the China Academy of Railway Sciences (CARS). The GPR signals of different frequencies and different coupling forms of antennas were collected. Suitable ballast layer detection antenna and application parameters (introduced in 2.3) were obtained based on the signal resolution and ability of distinguishing ballast-subgrade interface. In addition, to further verify the GPR applicability for ballast layer inspection in China (big area with complex environmental conditions), the data collected by the low-frequency GPR system mounted on the tunnel inspection vehicle was analysed. The corresponding relationship between ballast-subgrade interface and ballast layer maintenance was analysed.

Methodology

Full-scale ballasted track model

The ballasted track was built on a 30 m length and 3 m deep tank specifically for testing, where no train passes before and during the test. Therefore, the ballast and fouling materials will keep at the original position after construction. The subgrade is 2.3 m deep. The ballast layer width is 5 m. Mono-block concrete (Chinese Type III) is used. The rail is Type 60 (60 kg/m). The Class I ballast (highest level ballast) is used according to Chinese standard for ballast[50]. The ballast material is basalt, and ballast size ranges from 25 mm to 63 mm, referring to for detailed information on PSD and physical properties. No sub-ballast is added according to 1 type of the defined track bed structure in China standard.

The profile of the full-scale ballasted track model is shown in Fig. 1.

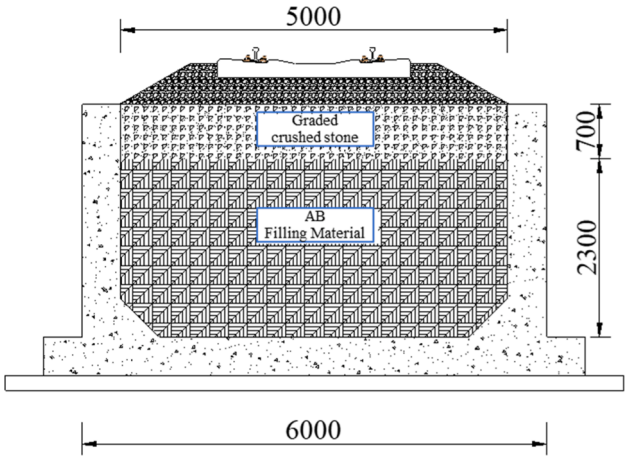

Fig. 1. Full-scale ballasted track model (unit: mm).

The full-scale ballasted track is divided into four sections, and each section is 7.5 m. Section I and Section II are highly fouled sections, which means all the voids in the ballast layer is filled by fouling. Section III is medium fouled, which means the fouled ballast layer thickness is 17 cm from the ballast layer bottom (ballast-subgrade interface). Section IV is clean section, which means no fouling in ballast layer of this section. Each section has one steel plate (size: 3.8 m long, 20 cm wide, 10 mm thick) at the ballast-subgrade interface. Their locations are recorded. The width of the steel plate is throughout the lateral direction of the track. The longitudinal section of the ballasted track and the steel plate locations are shown in Fig. 2.

The fouling material is crushed by stone crusher and sieved by square hole sieve to control the size of fouling particles. The fouling material in Section I was fine-grained coal with a particle size of less than 5 mm. The fouling material in Section II and Section III was small stones of basalt with a particle size of less than 7.1 mm. The full-scale ballasted track construction process is shown in Fig. 3. The ballast layer is constructed by placing the ballast and fouling with calculated mass in 2 layers. The ballast layer is constructed by placing the ballast and fouling of calculated mass in 2 layers. For each layer, ballast was firstly place and then is the fouling material. The weight of fouling material is controlled by the volume percent of 30 % for all fouling layers, the percent of mass content is calculated with their natural bulk densities (coal:1.2 g/mm^3, basalt: 2.8 g/mm^3) accordingly. Ballast fouling are distributed uniformly in lateral direction in track bed. Tamping was conducted after the placement of ballast and fouling for each layer. The fouling particles intrudes into the voids of ballast due to the vibration of tamper.

Before and after the construction of the full-scale ballasted track, the level meter was used to measure the heights of the ballast layer bottom and the top of rail at 10 locations, which is shown in Fig. 2. Then, the thickness of the ballast layer was calculated as shown in Table 1.

GPR system

The SIR30 4-channel data acquisition unit manufactured by GSSI was used. Three receiver antennas were used. Two of them are ground-coupled antennas with frequency at 400 MHz and 900 MHz, respectively. The last one is 2 GHz air-coupled antennas. The whole GPR system consists of antennas, master control units, recording and display terminals, distance encoders, etc. The system framework is shown in Fig. 4.

The GPR system was mounted on a metal-wheel trolley (named as inspection trolley), which moves by manpower. The GPR system together with the trolley (inspection trolley) are shown in Fig. 5a. In the Fig. 5a, the position of the three antennas can be seen. The 2 GHz antenna was put perpendicular to the track direction. The other two

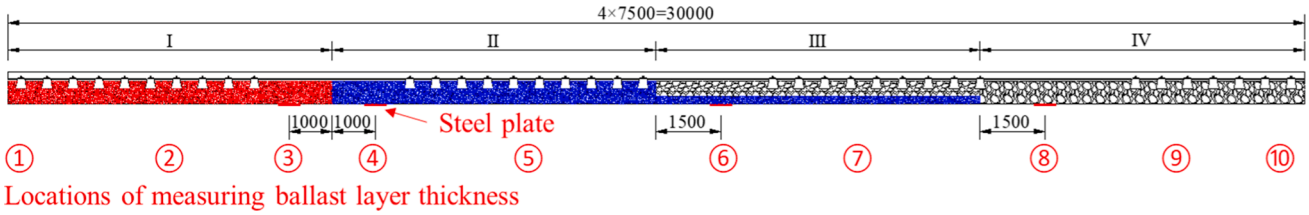

Fig. 2. Longitudinal section of full-scale ballasted track (unit: mm).

Fig. 3. Full-scale ballasted track construction process.

Table 1
Ballast layer thickness at 10 locations of full-scale ballasted track.

Measured location number	1	2	3	4	5	6	7	8	9	10
Ballast layer thickness (unit: cm)	38	40	37	36	36	33	38	39	43	40

antennas were put along the track direction. Three antennas are installed to inspection the center of crip area and the outside of rails respectively. The bilateral antennas are 190 mm away from the rails in horizontal direction. The antenna positions are shown in Fig. 6. The speed of pushing the inspection trolley was about 3 km/h.

GPR application parameters

We also considered the influence of different GPR application parameters on the identification of the different layers (clean ballast, fouled ballast and subgrade). The GPR application parameters include the time window, the sampling points and the channel spacing. Because different frequency antennas have the performance. We considered that the 400 MHz antenna should use 40 ns time window. 900 MHz antenna should use 30 ns time window. 2 GHz antenna should use 15 – 25 ns time window. The number of sampling points for each GPR signal is uniformly 512. Considering that the inspection train can run maximum speed of 160 km/h, the minimum channel spacing should be 5 cm. The acquisition process is not set gain adjustment.

Ballast layer dielectric constant

This section content is modified after our submitted review paper [7] to explain more about the dielectric constant of ballast layer.

The propagation of electromagnetic waves in a medium follows Maxwell's equations. In most cases ballast is non-magnetic. Then, the propagation of electromagnetic waves can be described by the following two equations with time as the variable.

$$\nabla E = -\mu \frac{\partial H}{\partial t} \tag{1}$$

$$\nabla H = \varepsilon \frac{\partial E}{\partial t} + \sigma E$$

where $\boldsymbol{E}$ is the electric field strength, $\boldsymbol{H}$ is the magnetic field strength,

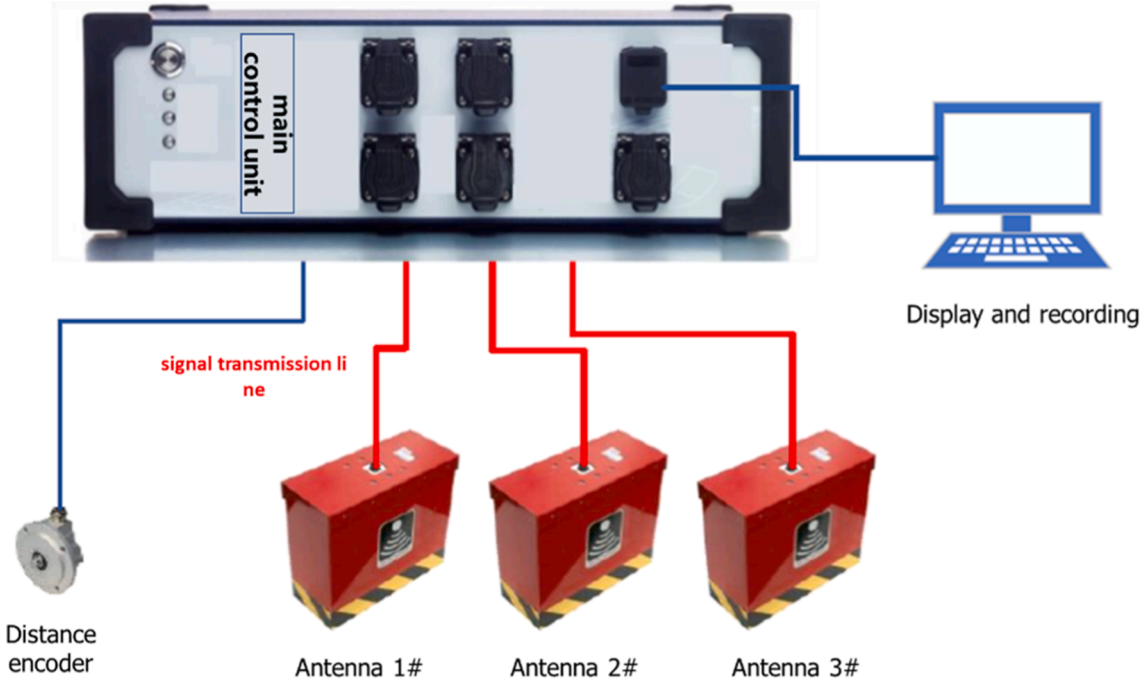

Fig. 4. Framework of the GPR system.

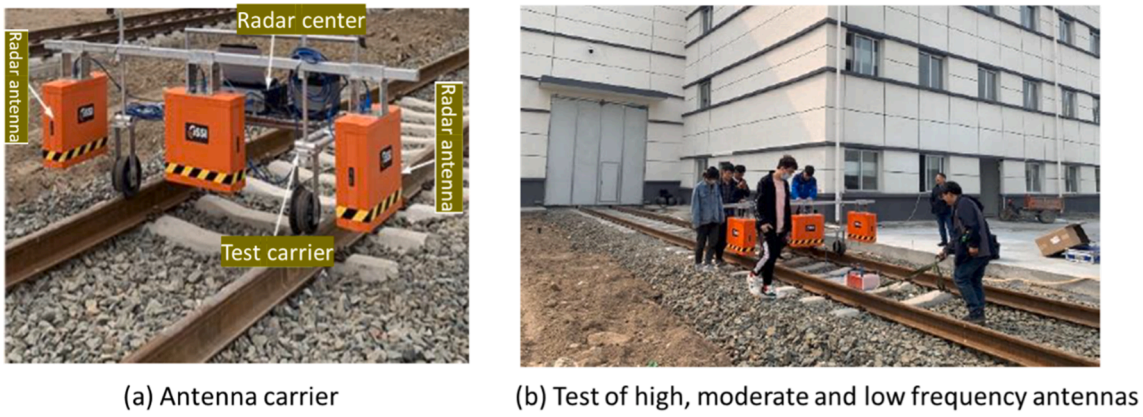

Fig. 5. GPR system and inspection trolley.

ε is the dielectric constant, μ is the magnetic permeability and σ is the electrical conductivity. ε, μ and σ are the three parameters that determine the propagation of electromagnetic waves in the ballast layer.

The dielectric constant ε characterizes the ability of a medium to be polarized by an electromagnetic field. The dielectric constant determines the speed of electromagnetic wave propagation (v) in the medium, as shown in Eq. (2):

$$v = \frac{c}{\sqrt{\varepsilon}} \tag{2}$$

Where, c is the propagation speed of electromagnetic waves in a vacuum (i.e. the speed of light). Electromagnetic wave propagation velocity in air is approximately the speed of light, which means the dielectric constant is close to 1. The dielectric constants of common materials in ballast layer is shown in Table 2. The dielectric constant of water is much larger than the other materials, and its dielectric constant is related to the frequency of electromagnetic wave. Because the magnetization ability of water in low-frequency electromagnetic field is strong, then the dielectric constant is high. While the phenomenon of Relax happens for water molecules in electromagnetic field, then the water magnetization ability is weak. Then, the water dielectric constant is low. Nevertheless, research shows that the Relax is not apparent at natural ambient temperature with the electromagnetic wave frequency at 2 GHz. The 2 GHz is the most popular frequency in the recent published papers [23,27,51].

Ballast layer is a mixture of ballast particles and the fouling contained within ballast voids. The dielectric constant of a mixed medium (consisting of two or more anisotropic materials) is usually calculated using the Complex Refractive Index Method (CRIM) [52], as shown in Eq. (3).

$$\varepsilon_b = \left(\sum \rho_i \varepsilon_i^{\alpha}\right)^{1/\alpha} \tag{3}$$

where ε_b is the dielectric constant of the mixture, ρ_i is the volume percentage of each material of the mixture, ε_i is the dielectric constant of each component, and α is a parameter that depends on the spatial structure and the angle between the mixture and the electric field, generally α is taken to be 0.5.

For example, there is a ballast layer with the porosity at 35 %. The dielectric constant of the fouled ballast layer can be calculated according

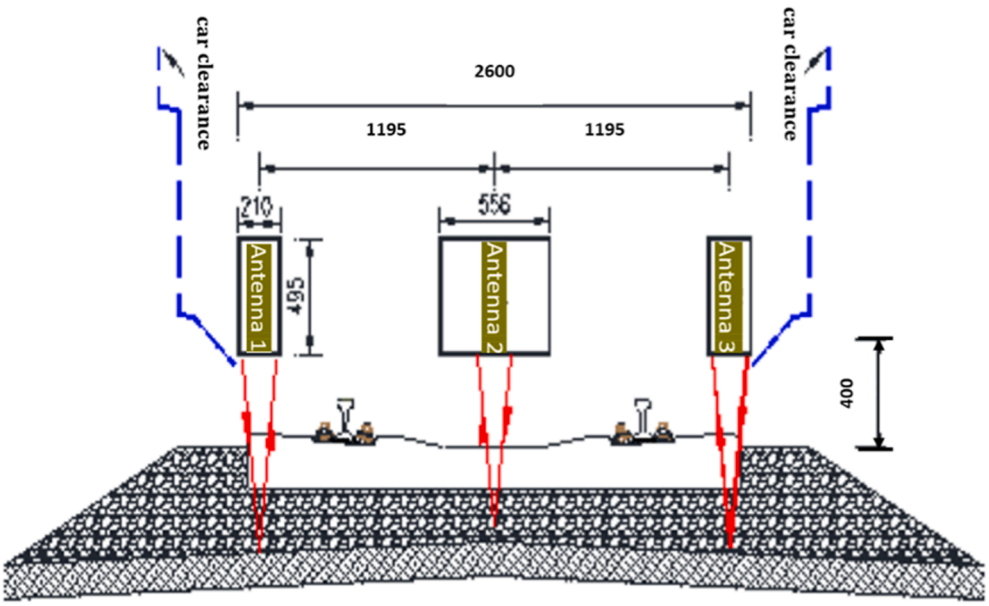

Fig. 6. Antenna setup, locations (unit: mm).

Table 2
Dielectric constants of common materials in ballast layer.

Ballast layer	Materials	Dielectric constant
Air	Air	≈ 1
Ballast	Granite	5–7
	Limestone	4–8
Fouling composition	Water	80 + (related to the wave frequency)
	Sands	3–6
	Soil	2–19
	Coal	3–4

to the CRIM (Equation (3)). The fouled ballast layer can be seen as one medium made by ballast, air, water and fine particles, etc. Considering water and fine particles filling ballast voids from 0 to 100 % respectively, the mixture dielectric constants are calculated as shown in Fig. 7. The gray level and the dielectric constant is presented in legend. When all the ballast voids were filled by water, the mixture dielectric constants increase from 4 to 22. When all the ballast voids are filled by fine particles, the mixture dielectric constants increase from 4 to 7. This means that water is the determining factor for the dielectric constant of the ballast layer.

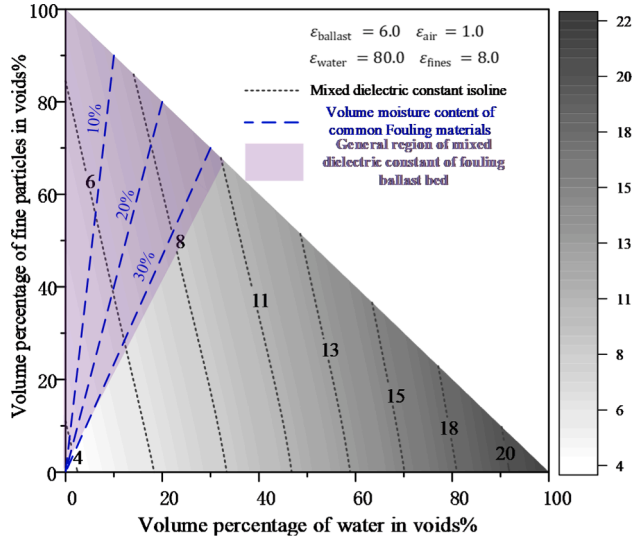

Fig. 7. Distribution of dielectric constants for ballast layers at different fouling levels.

In addition, Fig. 7 present the results in ideal condition, which assumes that the fine particles and water can exist independently in ballast void. But the water exists mainly relying on the fouling. The studies [53–56] show that the normal fouling material (mostly soil) in ballast layer can store less than 30 % water to the total fouling volume. The small ballast particles can contain water less than 20 %, and the loose fine particles of coal can hold water less than 10 %. The blue dash lines indicated the above-mentioned volume moisture content (10 %, 20 %, 30 %) of common fouling materials, and the dielectric constant is obtained accordingly. Therefore, the dielectric constants of fouled ballast layer usually distribute at the purple area in Fig. 7. Generally, the clean ballast layer dielectric constant is about 4, while the dielectric constants of top-fouled ballast layer (all voids are filled by fouling) are from 7 to 11, which depends on the water holding capacity of the fouling.

Magnetic permeability (μ in Eq. (1)) affects the speed of electromagnetic wave propagation and energy attenuation in a medium. The magnetic permeability of ballast and common fouling materials is generally low, for which this is usually not considered in earlier studies.

Electrical conductivity (σ in Eq. (1)) has a negligible effect on the speed of electromagnetic wave propagation in the medium, but it mainly triggers energy attenuation in signal transmission. The electrical conductivity is dependent on the electromagnetic wave frequency, but in the range of the GPR signal band (MHz - GHz), electrical conductivity influence on the results can also be ignored.

Results and discussions

Detection depth of 2 GHz air-coupled antenna

In order to test the effect of different time windows on the GPR detection depth, the 30 m ballasted track was tested by the GPR with two time windows of 15 ns and 20 ns. The radar images of the three locations using different time windows (15 ns and 20 ns) are shown in Fig. 8. The three locations are the Location 1, Location 2 and Location 3 in the Fig. 2.

The test results show the two time windows both can effectively receive the reflected signal at the bottom of the ballast layer (ballast-subgrade interface), as proved in Fig. 8. The blue marks are the

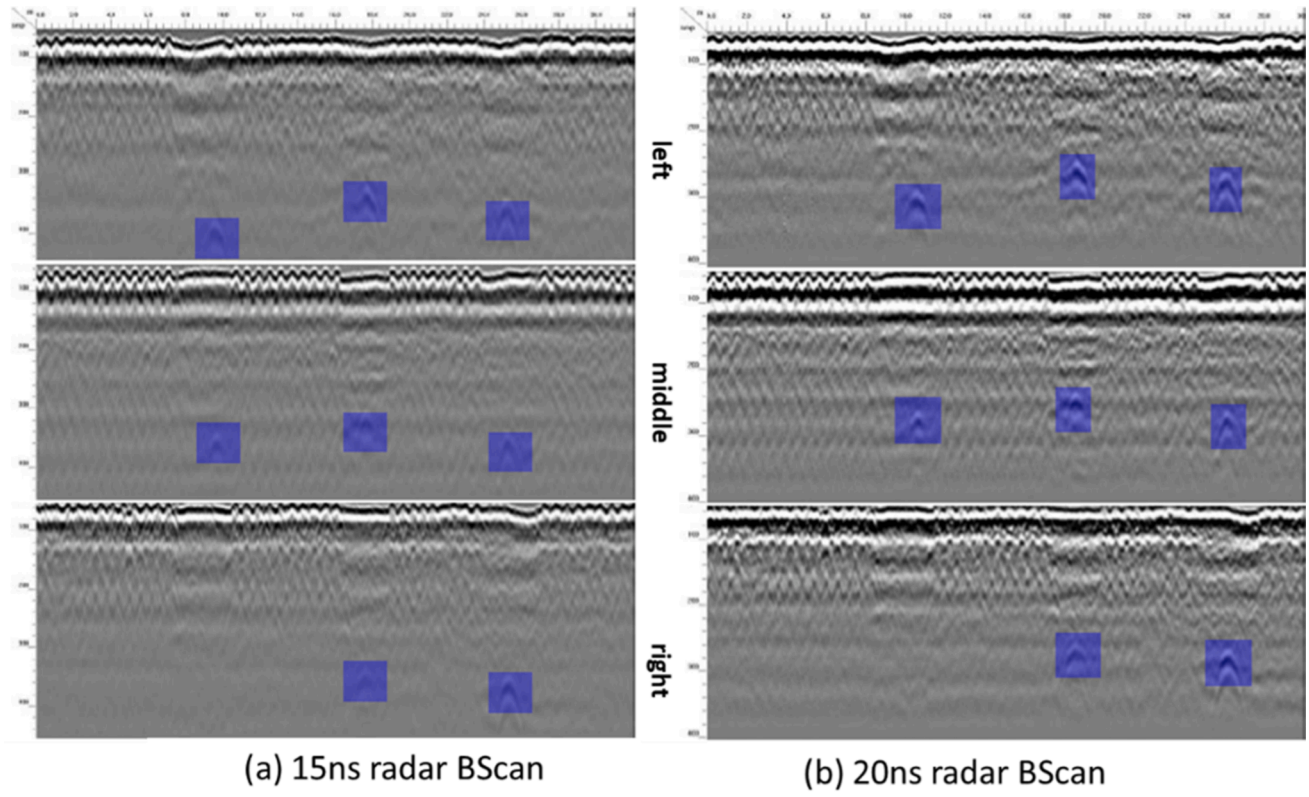

Fig. 8. Detection depth results of different GPR time windows.

reflection from the steel plates, which were put at the ballast-subgrade interface (introduced in Section 2.1). The dielectric constant is obtained in dry condition by the pre-placed steel plate under the ballast layer. The placement of steel plate also contributed to verify the results from other researchers, as well to help for the identification of ballast layer in dry condition for the field test in the followed sections of this paper. Results also indicate that the effective detection depth of the 2 GHz GPR system is greater than 45 cm (from the sleeper bottom), and

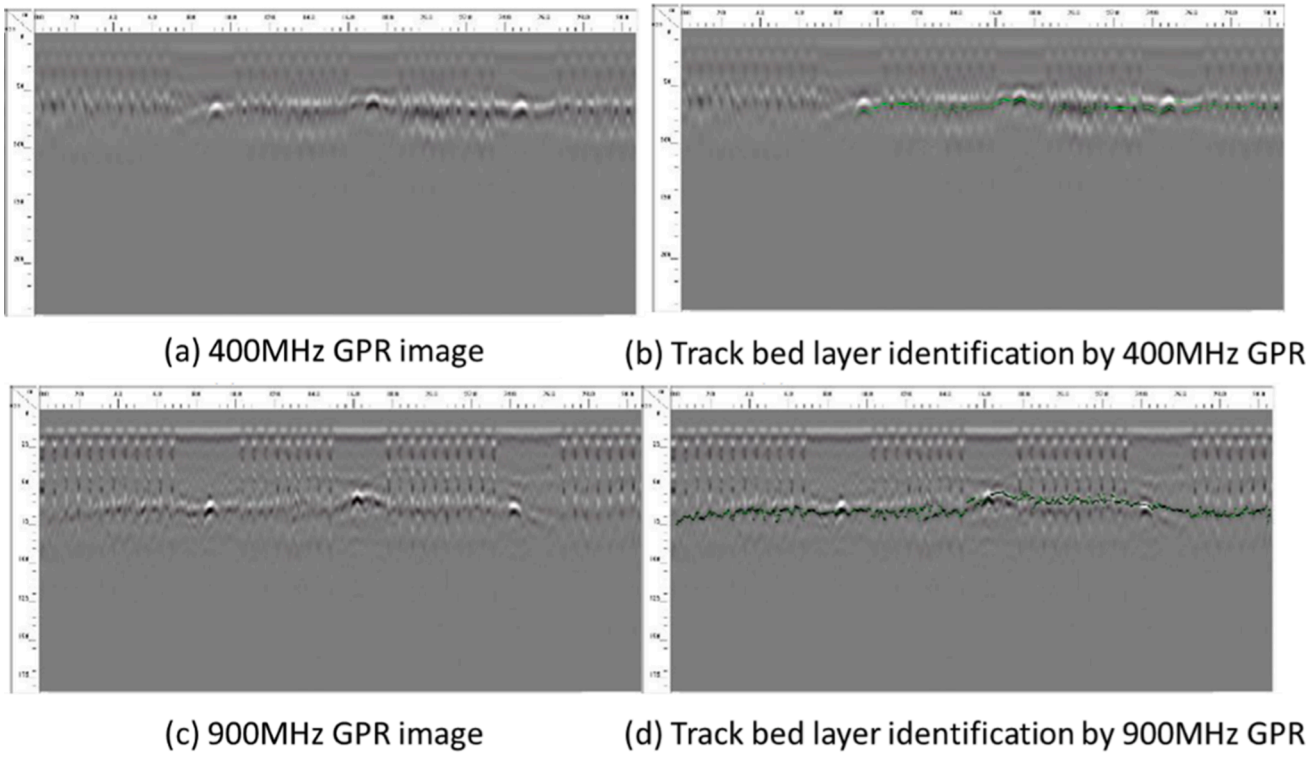

Fig. 9. GPR images of 400 MHz and 900 MHz antennas and layer interface.

the effective detection depth is greater than 65 cm (from ballast layer top surface). This can cover the whole depth of ballast layer, which means it can meet the needs of ballast layer detection. For the 15 ns time window, the detection depth is closely below the steel plate. This means the proportion of effective data (for ballast layer) in a single waveform is greater, which is easier to analyse the ballast layer condition.

Effect of ground-coupled low and medium frequency antenna layers revealed

The GPR images and layer interface results of the ground-coupled antennas (400 MHz and 900 MHz) are shown in Fig. 9. It can be seen from the figure that there is a strong reflection signal at each pre-buried steel plate at the bottom of the roadbed, and there is a continuous reflection interface along the bottom of the roadbed in the longitudinal direction, and the ground-coupled antenna has excellent layer identification capability.

Signal characteristics of antennas at different frequencies

The signal characteristics of antennas at different frequencies are shown in Fig. 10. The signal axis crossings (i.e. the crossings of signal amplitude curve and the coordinate axis in the ballast layer indicated by red points in square box) of the 400 MHz frequency antenna is significantly less than that of the 2 GHz antenna. The 900 MHz axis crossings are also less than 2 GHz axis crossings. This means the signal (time-domain and frequency-domain) characteristics (to reflect ballast layer information) of the 2 GHz antenna has better performance than the 400 MHz and 900 MHz antennas.

Dielectric constants for different ballast fouling levels

Using the locations with clear signal reflections (blue marks in Fig. 8), the peak reflections from the ballast layer surface and steel plate at the same location were picked up in the GPR image. Then, the return travel time was calculated. Combining with the ballast thickness results (Table 1), the dielectric constants are calculated using Eq. (4). The dielectric constant results using GSSI SIR30 are shown in Table 3.

Table 3
Dielectric constant results for different sections (400 MHz antenna).

Track location	Section	Return time (ns)	Distance (cm)	Dielectric constant
Right sleeper end	II	9.2	52	7.0
	III	7.4	51	4.8
	IV	8.1	56	4.7
Crib ballast	II	8.4	50	6.4
	III	7.2	52	4.3
	IV	8.4	58	4.7
Left sleeper end	III	8.2	55	5.0
	IV	8.7	60	4.7

$$\varepsilon_r = \left(\frac{c\Delta t}{2h}\right)^2 \quad (4)$$

In Eq. (4), ε_r is the dielectric constant; c is the speed of electromagnetic wave propagation in vacuum; Δt is the return travel time of the electromagnetic wave in the medium; h is the distance between the ballast layer surface and the steel plate.

The test results show that the dielectric constants of Section II (highly fouled ballast) range from 6.4 to 7.0 with an average value of 6.7. The dielectric constants of section III (medium fouled ballast) range from 4.3 to 5.0 with an average value of 4.7. The dielectric constants of section IV (clean ballast) are more uniform with an average value of 4.7. The average dielectric constant value of Section II (highly fouled ballast) is the largest, while average dielectric constant values of the Section III and Section IV are the same. But there is some dispersion in the section III dielectric constants. This indicates that the clean bed dielectric constant is relatively uniform. The dielectric constant increases as the fouling level increases. The test results are consistent with the results of the CRIM model as shown in Fig. 7.

400 MHz GPR field inspection results

The objective is to test the ability of the 400 MHz antenna to identify the clean ballast thickness, further testing the 400 MHz GPR application feasibility on the field ballast layer inspection. Two railway lines were

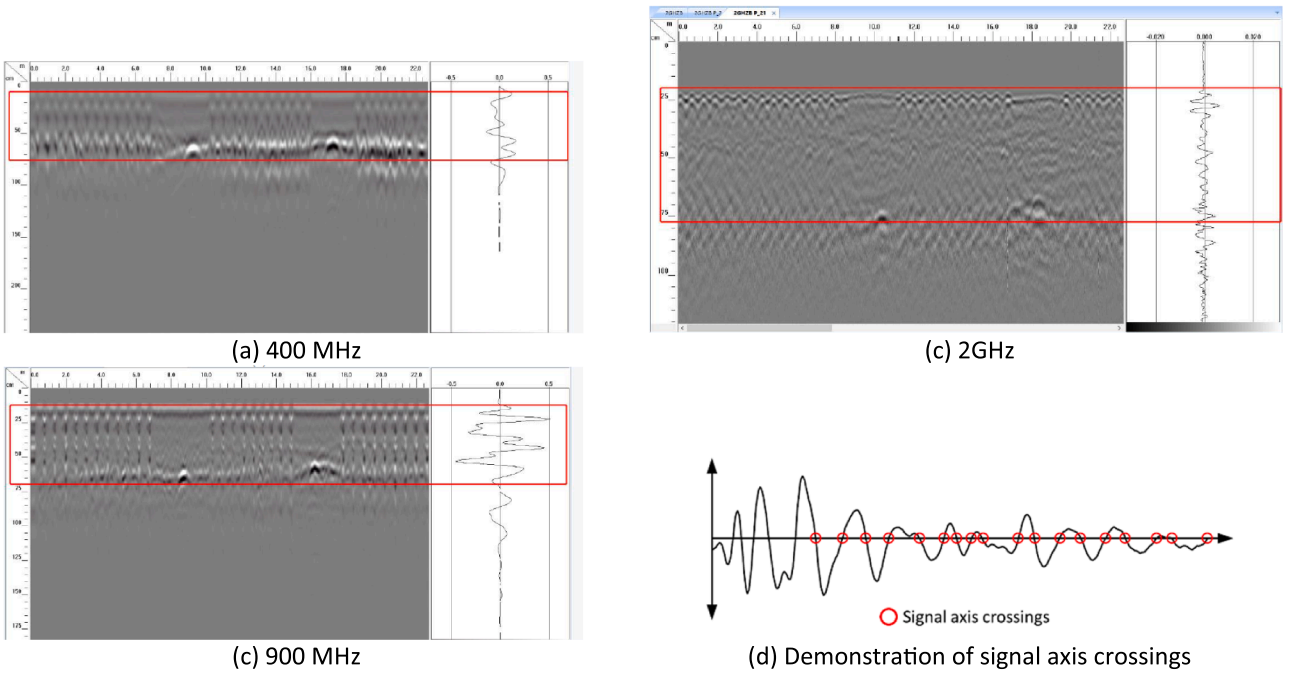

Fig. 10. Signal characteristics of antennas at different frequencies.

inspected by the GPR system. One is named as Line #1 with the measured length as of 600 km. The other is named as Line #2 with the measured length about 80 km. The two lines were inspected in April 2019.

The results show that the clean-fouled ballast interface in the ballast layer of the Line #1 is very clear. The clean ballast layer decreases gradually with the increase of the cleaning time, as shown in Fig. 11. Differently, in Fig. 12, the clean-fouled ballast interface in the ballast layer of the Line #2 (in the northern China) is not clear, and some of the clean ballast thicknesses are beyond the ballast layer thickness (50 cm). The main reason causing the clean ballast layer thickness difference is that the Line #1 is in a humid and rainy region, while the Line #2 is a dry and cold region. From the results, we concluded that using the 400 M antenna to measure the clean ballast layer thickness have clear limitations at the accuracy and reliability. In addition, the antenna vertical resolution is about 75 mm, which cannot clearly present the ballast layer GPR images. Because the ballast particle size is in the range of 20–60 mm, mostly around 30–40 mm, and the resolution 75 mm is bigger than ballast particle size.

Another reason that proves the 400 MHz antenna is not suitable for field ballast layer inspection is explained as follows. The Line #2 GPR inspection results (Fig. 12) show that clean ballast layer thickness increases with the increase of the service time. This is contrary to the objective law, which is ballast layer deteriorates with the of service time. In addition, the ballast layer thicknesses of Year 2011 and Year 2017 are around 40 – 50 cm, which is thicker than normal ballast thickness. This means the 400 MHz antenna cannot distinguish the interface of clean-fouled ballast. Because the reflection at the interface of clean-fouled ballast is not strong, but the reflection at the ballast-subgrade interface (where has large dielectric constant difference) is strong. Therefore, it is not suitable to use 400 MHz GPR to inspect ballast layer condition in dry cold regions.

AAA 2 GHz GPR field inspection results

In order to further verify the inspection capability of 2 GHz antennas on operational field railway lines, the Line #3 (railway line name) was selected for our field study. The inspected railway line was 450 m long, which contains different forms of sub-structure, including subgrade, bridges and tunnels. The ballast layers on the subgrade and bridges in the inspected section had not been cleaned in the past 15 years. The phenomenon of mud-pumping was serious. For the ballast layer in the tunnel was manually cleaned 6 months before the inspection. The GPR system and parameters used in the field inspection is consistent with those used for the 30 m full-scale track. The 2 GHz antenna was used. The time window is 15 ns. The channel spacing is 5 cm. The l typical location of the ballast layer on the subgrade was drilled for fouled ballast samples. The drilled hole was deep to the subgrade surface. The inspected section layout and test results are shown in Fig. 13.

From the test results it can be seen that.

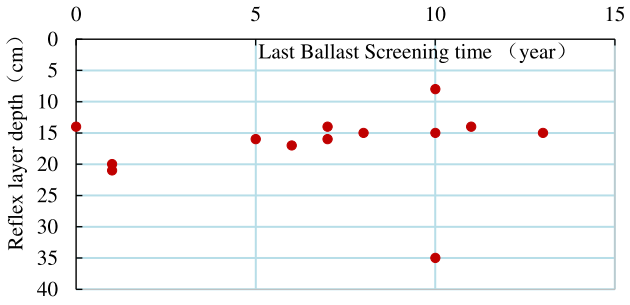

Fig. 11. Correlation between clean ballast layer thickness and ballast cleaning years in Line #1.

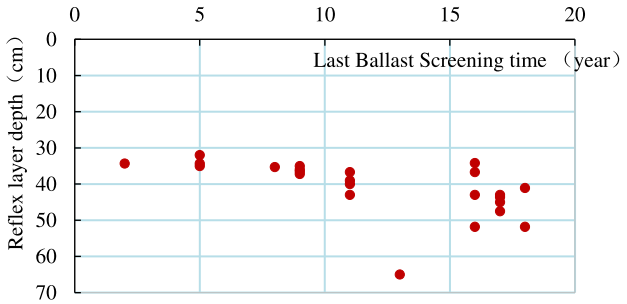

Fig. 12. Correlation between clean ballast layer thickness and ballast cleaning years in Line #2.

(1) The ballast/sub-structure interface can be seen clearly at the sub-structures of bridge and subgrade in the inspected section. No clear interfaces at ballast-tunnel were seen in the tunnel section.
(2) The drilled hole is 53 cm from ballast layer surface to the subgrade top surface. The return time of the signal is about 8.7 ns. The ballast thickness under the sleeper is 30 cm. The dielectric constant is 6.0. The GPR reflection signals (ballast-tunnel interface) before and after the drilled hole are clear. Compared to the clean section of the 30 m full-scale ballasted track, the dielectric constant is significantly increased, indicating ballast layer is seriously fouled.
(3) The inspected bridge section has the serious mud-pumping phenomenon. But the interface of the ballast layer and the *T*-beam surface is still clear (the original GPR data was performed a slight gain). This means even at the highly fouled ballast layer locations (with mud-pumping), the 2 GHz GPR can still cover the enough detection depth, which is 30 cm under the sleeper. This proves the 2 GHz GPR can be used for rapid inspection of ballast layer (regarding the fouling level).

Conclusions

This paper combined the experimental tests and the field tests/measurements. For the experimental tests, we built a 30 m long full-scale ballasted track for testing the GPR. In addition, the antennas and GPR parameters were confirmed for the field tests. For the field tests, three railway lines were inspected with the GPR (different antennas, 400 MHz and 2 GHz). A hole on the ballast layer was drilled to verify the GPR results. By performing this study, the following conclusions can be given.

1. Ballast layer inspection should be performed mainly with the 2 GHz antenna and supplemented by the 400 MHz and 900 MHz antennas.
2. The GPR inspection results (on full-scale track and field railway line) both show that the effective detection depth of 2 GHz GPR is not less than 65 cm, which can meet the needs of ballast layer inspection.
3. 2 GHz GPR parameters for ballast layer can be set at 5 cm channel spacing, 512 sampling points and 15 ns time window.
4. The dielectric constants of clean ballast layer are relatively uniform, with a result of 4.7 (average) in the dry condition. The dielectric constant increases significantly with the increase of the fouling level.

CRediT authorship contribution statement

Guixian Liu: Funding acquisition, Resources, Writing – review & editing. **Zhan Peng:** Formal analysis, Investigation. **Guoqing Jing:** Supervision. **Shilei Wang:** Formal analysis, Investigation, Software, Visualization, Funding acquisition. **Yaonan Li:** Formal analysis, Validation. **Yunlong Guo:** Writing – original draft, Writing – review & editing.

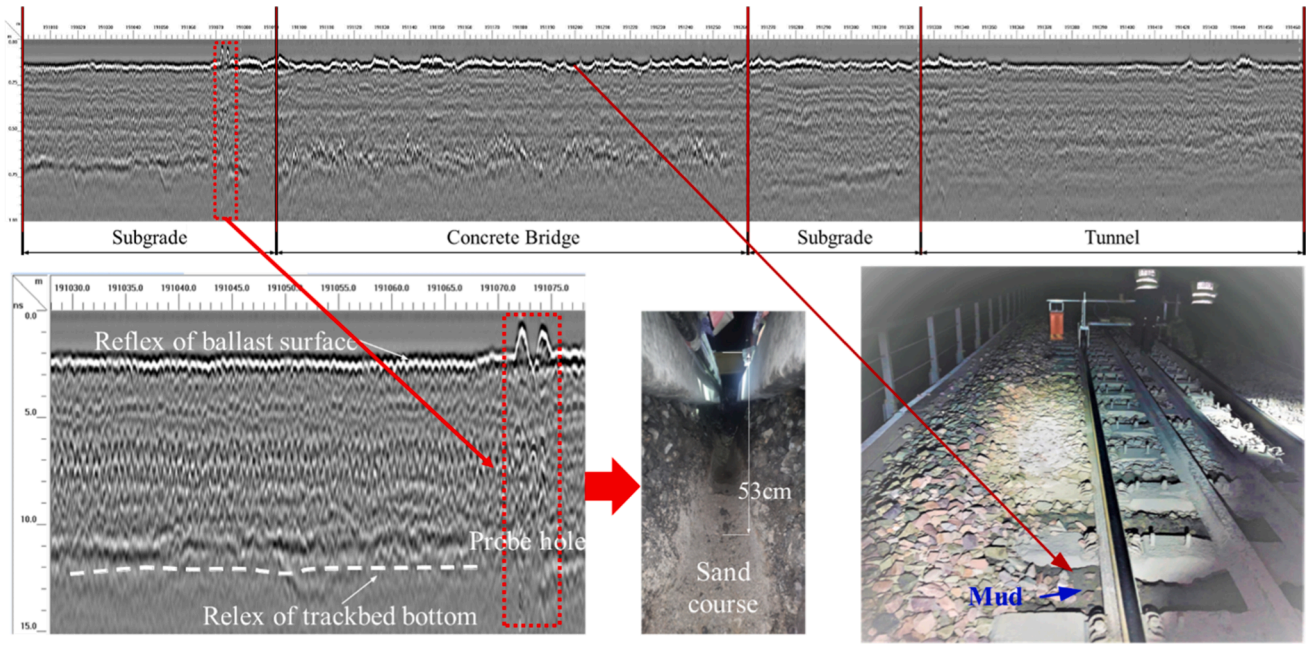

Fig. 13. Inspected section layout and inspection results of 2 GHz GPR.

Declaration of Competing Interest

The authors declare that they have no known competing financial interests or personal relationships that could have appeared to influence the work reported in this paper.

Acknowledgements

This research is funded by the key research and development project of China Academy of Railway Sciences Corporation Limited (2021YJ251).

References

[1] Zhai W. Vehicle–track coupled dynamics theory and applications. Singapore: Springer; 2020.
[2] Selig ET, Waters JM. Track geotechnology and substructure management. Thomas Telford 1994.
[3] Tutumluer E, Qian Y, Hashash YMA, Ghaboussi J, Davis DD. Discrete element modelling of ballasted track deformation behaviour. International Journal of Rail Transportation 2013;1(1–2):57–73.
[4] Indraratna B, Salim W, Rujikiatkamjorn C. Advanced rail geotechnology: Ballasted track. CRC Press London; 2011.
[5] Li D, Hyslip J, Sussmann T, Chrismer S. Railway geotechnics. CRC Press; 2002.
[6] Sabato A, Niezrecki C. Feasibility of digital image correlation for railroad tie inspection and ballast support assessment. Measurement 2017;103:93–105.
[7] Wang S, Liu G, Jing G, Feng Q, Liu H, Guo Y. State-of-the-Art Review of Ground Penetrating Radar (GPR) Applications for Railway Ballast Inspection. Sensors 2022; 22(7):2450.
[8] Guo Y, Wang S, Jing G, Yang F, Liu G, Qiang W, et al. Assessment of ballast layer under multiple field conditions in China. Constr Build Mater 2022;340:127740.
[9] Guo Y, Liu G, Jing G, Qu J, Wang S, Qiang W. Ballast fouling inspection and quantification with ground penetrating radar (GPR). International Journal of Rail Transportation 2022:1–18.
[10] Xu L, Zhai W. Train–track coupled dynamics analysis: system spatial variation on geometry, physics and mechanics. Railway Engineering Science 2020:1–18.
[11] Bakhtiary A, Zakeri JA, Mohammadzadeh S. An opportunistic preventive maintenance policy for tamping scheduling of railway tracks. International Journal of Rail Transportation 2021;9(1):1–22.
[12] Indraratna B, Ngo NT, Rujikiatkamjorn C. Behavior of geogrid-reinforced ballast under various levels of fouling. Geotext Geomembr 2011;29(3):313–22.
[13] Guo Y, Markine V, Jing G. Review of ballast track tamping: Mechanism, challenges and solutions. Constr Build Mater 2021;300.
[14] Huang H, Tutumluer E. Discrete Element Modeling for fouled railroad ballast. Constr Build Mater 2011;25(8):3306–12.
[15] Sadeghi J, Motieyan Najar ME, Zakeri JA, Kuttelwascher C. Development of railway ballast geometry index using automated measurement system. Measurement 2019;138:132–42.
[16] Chang C, Ling L, Chen S, Zhai W, Wang K, Wang G. Dynamic performance evaluation of an inspection wagon for urban railway tracks. Measurement 2020.
[17] S. Schmidt, S. Shah, M. Moaveni, B.J. Landry, E. Tutumluer, C. Basye, D. Li, Railway Ballast Permeability and Cleaning Considerations, Transportation Research Record: Journal of the Transportation Research Board (2607) (2017) 24-32.
[18] Fortunato E, Pinelo A, Fernandes MM. Characterization of the fouled ballast layer in the substructure of a 19th century railway track under renewal. Soils Found 2010;50(1):55–62.
[19] Kuo C. Ground-penetrating radar to investigate mud pumping distribution along a railway line. Constr Build Mater 2021;290.
[20] Mishra D, Qian Y, Huang H, Tutumluer E. An integrated approach to dynamic analysis of railroad track transitions behavior. Transp Geotech 2022;1(2):188–200. In this issue.
[21] De Bold R, O'Connor G, Morrissey JP, Forde MC. Benchmarking large scale GPR experiments on railway ballast. Constr Build Mater 2015;92:31–42.
[22] Liu J, Cheng YS. A New Approach of Detecting and Evaluation Railway by Using the Train-Mounted Ground Penetrating Radar in China. Advanced Materials Research 2011;243-249:4351–5.
[23] Scanlan KM, Hendry MT, Martin CD, Schmitt DR. A Review of Methods for Estimating Ballast Degradation Using Ground-Penetrating Radar. Railroad Ballast Testing and Properties 2018:54–76.
[24] Eriksen A, Gascoyne J, Fraser R. Ground penetrating radar as part of a holistic strategy for inspecting trackbed. Aust Geomech Soc 2011;46(3):1–11.
[25] Benedetto A, Tosti F, Bianchini Ciampoli L, Calvi A, Brancadoro MG, Alani AM. Railway ballast condition assessment using ground-penetrating radar – An experimental, numerical simulation and modelling development. Constr Build Mater 2017;140:508–20.
[26] Anbazhagan P, Lijun S, Buddhima I, Cholachat R. Model track studies on fouled ballast using ground penetrating radar and multichannel analysis of surface wave. J Appl Geophys 2011;74(4):175–84.
[27] Al-Qadi I, Xie W, Roberts R. Optimization of antenna configuration in multiple-frequency ground penetrating radar system for railroad substructure assessment. NDT and E Int 2010;43(1):20–8.
[28] Artagan SS, Borecky V. Advances in the nondestructive condition assessment of railway ballast: A focus on GPR. NDT and E Int 2020;115.
[29] De Chiara F, Fontul S, Fortunato E. GPR Laboratory Tests For Railways Materials Dielectric Properties Assessment. Remote Sensing 2014;6(10):9712–28.
[30] Bianchini Ciampoli L, Tosti F, Economou N, Benedetto F. Signal Processing of GPR Data for Road Surveys. Geosciences 2019;9(2).
[31] Shao W, Bouzerdoum A, Phung SL, Su L, Indraratna B, Rujikiatkamjorn C. Automatic classification of ground-penetrating-radar signals for railway-ballast assessment. IEEE Trans Geosci Remote Sens 2011;49(10):3961–72.
[32] Al-Qadi IL, Xie W, Roberts R. Scattering analysis of ground-penetrating radar data to quantify railroad ballast contamination. NDT and E Int 2008;41(6):441–7.
[33] Tosti F, Bianchini Ciampoli L, Calvi A, Alani AM, Benedetto A. An investigation into the railway ballast dielectric properties using different GPR antennas and frequency systems. NDT and E Int 2018;93:131–40.
[34] Shangguan P, Al-Qadi IL, Leng Z. Ground-Penetrating Radar Data to Develop Wavelet Technique for Quantifying Railroad Ballast-Fouling Conditions. Transportation Research Record: Journal of the Transportation Research Board 2012;2289(1):95–102.

[35] C. Basye, S.T. Wilk, Y. Gao, Ground Penetrating Radar (GPR) Technology and Evaluation Implementation, United States. Department of Transportation. Federal Railroad Administration, 2020.
[36] Brown M, Li D. Ground penetrating radar technology evaluation and implementation: phase 2, United States. Federal Railroad Administration Office of Research … 2017.
[37] Eriksen A, Gascoyne J, Mangan C, Fraser RJCR. Rejuvenation, Renaissance, Practical applications of GPR surveys for trackbed characterisation in the UK. Ireland: USA and Australia; 2010. p. 380.
[38] D. Read, A. Meddah, D. Li, W. Mui, Ground penetrating radar technology evaluation on the High Tonnage Loop: phase 1, 2017.
[39] R. Roberts, I. Al-Audi, E. Tutumluer, J. Boyle, Subsurface Evaluation of Railway Track Using Ground Penetrating Radar, (2008).
[40] Sadeghi J, Motieyan-Najar ME, Zakeri JA, Yousefi B, Mollazadeh M. Improvement of railway ballast maintenance approach, incorporating ballast geometry and fouling conditions. J Appl Geophys 2018;151:263–73.
[41] Narayanan RM, Jakub JW, Li D, Elias SEG. Railroad track modulus estimation using ground penetrating radar measurements. NDT and E Int 2004;37(2):141–51.
[42] Roberts R, Rudy J, Al-Qadi I, Tutumluer E, Boyle J. Railroad ballast fouling detection using ground penetrating radar–a new approach based on scattering from voids. Ninth European Conference on NDT, Citeseer 2006.
[43] Fontul S, Fortunato E, De Chiara F, Burrinha R, Baldeiras M. Railways Track Characterization Using Ground Penetrating Radar. Procedia Eng 2016;143:1193–200.
[44] Kuo C, Hsu C, Chen Y, Wu C, Wang H, Chen D, et al. Using Ground-penetrating Radar to Promote the Investigating Efficiency in Mud Pumping Disaster of Railways. Proceedings of Engineering and Technology Innovation 2016;4:49.
[45] Silvast M, Nurmikolu A, Wiljanen B, Levomaki M. An Inspection of Railway Ballast Quality Using Ground Penetrating Radar in Finland. Proceedings of the Institution of Mechanical Engineers, Part F: Journal of Rail and Rapid Transit 2010;224(5):345–51.
[46] Bianchini C. Calvi, D'Amico, Railway Ballast Monitoring by Gpr: A Test Site Investigation. Remote Sensing 2019;11(20):2381.
[47] Ciampoli LB, Calvi A, Oliva E. Test-site operations for the health monitoring of railway ballast using Ground-Penetrating Radar. Transp Res Procedia 2020;45:763–70.
[48] Clark M, Gillespie R, Kemp T, McCann D, Forde M. Electromagnetic properties of railway ballast. NDT and E Int 2001;34(5):305–11.
[49] Wang Z, Jing G, Yu Q, Yin H. Analysis of ballast direct shear tests by discrete element method under different normal stress. Measurement 2015;63:17–24.
[50] T.P.M.o. Railways, Railway Ballast, TB/T2140-2008, China Railway Publishing House, Beijing, 2008.
[51] R. Roberts, I. Al-Qadi, E. Tutumluer, Track Substructure Characterization Using 500 MHz and 2 GHz Ground Penetrating Radar: Results from over 250 Miles of Track in Wyoming and Alaska, Urbana 51 61801.
[52] Liao H, Sun J, Zan Y, Zhu Q, Gui F. Dielectric constant model for soil and its application in engineering. Chin J Geotech Eng 2016;38(S2):36–41.
[53] Trinh VN, Tang AM, Cui Y-J, Dupla J-C, Canou J, Calon N, et al. Mechanical characterisation of the fouled ballast in ancient railway track substructure by large-scale triaxial tests. Soils Found 2012;52(3):511–23.
[54] Rusong N, Wuming L. Physical and mechanical properties of mud pumping soils in railway subgrade bed. Journal of Southwest Jiaotong University 2018;53(2).
[55] Liu B, Su Q, Pham D, Bai H, Lamthi H. Study of critical dynamic stress and deformation law of graded gravel under different moisture content. Tiedao Xuebao/Journal of the China Railway Society 2016;38(6):100–7.
[56] Wang C, Gao Y, Guo C, Wei K. Experimental study on the influence of moisture content on soft coal strength characteristics. International Journal of Mining Mineral Engineering 2021;12(3):163–80.